Phys. Status Solidi B **250,** No. 2, 244–248 (2013) / **DOI** 10.1002/pssb.201200524

physica status solidi b
www.pss-b.com
basic solid state physics

The effect of Ga-doping on the defect chemistry of $RE_3Al_5O_{12}$ garnets

C. R. Stanek*[,1], C. Jiang[2], S. K. Yadav[1,3], K. J. McClellan[1], B. P. Uberuaga[1], D. A. Andersson[1], and M. Nikl[4]

[1] Los Alamos National Laboratory, Los Alamos, NM 87545, USA
[2] University of Wisconsin, Madison, WI 53706-1595, USA
[3] University of Connecticut, Storrs, CT 06269-3136, USA
[4] Institute of Physics AS CR, Prague 162 53, Czech Republic

Received 23 July 2012, accepted 3 December 2012
Published online 28 January 2013

Keywords aluminate garnets, antisite defects, Ga doping

* Corresponding author: e-mail stanek@lanl.gov, Phone +1 505 664 0361, Fax: +1 505 665 9062

It has been recently shown that the addition of Ga to $Lu_3Al_5O_{12}$ garnet (LuAG) removes the electron trapping associated with cation antisite defects. In this paper, we show via atomic scale simulations that the replacement of Al with Ga in LuAG actually lowers the energy of the antisite disorder process. Thus, we predict that Ga additions will lead to an increase of the antisite defect concentration and, in the absence of the electronic structure changes, would actually degrade the performance of the material. Since there are two crystallographically distinct Al sites in the garnet structure, we not only present results for complete replacement of Al with Ga, but also partial replacement for 40% (on 16a) and 60% (on 24d) of the Al with Ga. Our results support the explanation for Ga-doping leading to improvement in garnet scintillator performance that relies on variations of the electronic structure rather than reduction of the antisite defect concentration.

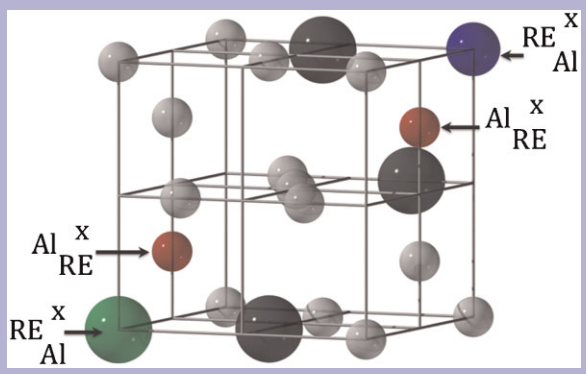

Cation antisite defects in $RE_3Al_5O_{12}$ garnet, where small light gray atoms and large dark gray atoms are lattice Al and RE atoms, respectively. The constituents of the antisite defect pairs are labeled, and it should be noted that the Ga atom (blue) is similar in size to RE (green). Oxygen atoms are not shown for clarity.

1 Introduction For some time, cation antisite defects (e.g., Y^{3+} on Al^{3+} sites in $Y_3Al_5O_{12}$) have been proposed as predominant defects [1–3] in aluminate garnets and more recently attributed as the origin of delayed scintillation response in these materials [4]. Furthermore, defects of this type have not only been predicted via atomic scale simulation to be the low energy intrinsic defect present in a range of aluminate garnets [5–7], but also the product of extrinsic defect processes such as aliovalent doping [8] and non-stoichiometry [9]. With regards to scintillator performance, after having identified antisites as a defect that limits performance (especially the timing characteristics), the next step is to attempt to remove these defects, or if that is not practical, at least their effects. In this paper, we focus our attention on recent experiments that revealed the presence of cation antisites via thermally stimulated luminescence (TSL) [10], and subsequently demonstrated a reduction in TSL peak (associated with antisites) height and a decrease in response time after Ga-doping [11].

The purpose of this paper is to employ atomic scale simulations to better understand the effect of Ga^{3+}-doping on the cation antisite defect chemistry in aluminate garnets.

In a previous paper, we showed through similar atomic scale simulations that Ga^{3+}-doping leads to changes in the electronic structure of aluminate garnets [12]. In that paper, we alluded to the fact that Ga doping could not lead to a reduction in the number of antisite defects. Here, we provide detail on that result, and focus on the impact of Ga^{3+}-doping on the concentration of cation antisite defects in aluminate garnets. Specifically, we show that the antisite defect reaction energy is lowered by Ga^{3+}-doping, thus leading to an increase in the antisite concentration. In support of this conclusion, it has recently been proposed that yttrium gallium garnet (YGG) has more antisites than YAG [13, 14], which is sensible since Ga^{3+} is closer in size to Y^{3+} (or any other RE^{3+}) than Al^{3+} [15]. Thus, variations of the electronic structure should be responsible for improved aluminate garnet scintillation performance rather than a reduction in the antisite concentration. We also describe associated details of the Ga^{3+}-doping process, including the site preference of Ga^{3+} on the two aluminum sites in YAG, namely: 16*a* and 24*d*, where the chemical formula accounting for these sites can be expressed as: $Y_3^{24c}\,Al_2^{16a}\,Al_2^{24d}\,O_{12}$.

2 Methodology Several atomistic simulation methods were employed in this work. For most of the antisite energetic calculations, we used a Born-like, ionic description of the lattice [16] and the Buckingham potential [17] to describe the short-range interactions between ions. All potential parameters were previously derived and can be found elsewhere: O^{2-}–O^{2-} by Grimes and Binks [18] and the remainder by Levy et al. [19] (though all were derived in the same self-consistent manner). Further information on these methods can be found elsewhere [20]. For spot checking pair potential calculations, as well as investigating the site preference of Ga in detail, we used density functional theory (DFT). Calculations were performed using the all-electron projector augmented wave method within the generalized gradient approximation (PAW-GGA), as implemented in the Vienna *ab initio* simulation package (VASP) [21]. Details can be found elsewhere [12].

3 Results

3.1 Antisite disorder mechanisms To begin our consideration of the effect of Ga^{3+}-doping on antisite defects in YAG and LuAG, we relied exclusively on lattice statics techniques to calculate the energy of each possible antisite disorder reaction. The relative energies of these reactions correspond to the relative concentration of defects present and therefore provide a qualitative picture of the effect of Ga^{3+}-doping on the overall antisite concentration. For example, Table 1 consists of the energies calculated for the antisite reactions possible for $x=0$ or $x=5$ in $Lu/Y_3Al_{5-x}Ga_xO_{12}$, i.e., compositions that contain all Al^{3+} (YAG and LuAG) or all Ga^{3+} (YGG and LuGG). Each reaction is expressed in Kröger–Vink notation [22], though all antisite defects here are charge neutral, and standard notation for charge has been omitted for brevity. Since there are two Al^{3+} or Ga^{3+} sites (16*a* and 24*d*), there are two reactions for each composition provided in Table 1. For all compositions, the 16*a* site is preferred by Lu^{3+} and Y^{3+} to the 24*d*, which agrees with previous pair potential studies [5–7]. This site preference is more pronounced for YAG and YGG than LuAG and LuGG, which is likely due to a size effect since Y^{3+} is larger than Lu^{3+} (1.019 Å vs. 0.977 Å, respectively, for VIII-fold ionic radii [15]) and the 16*a* octahedral site provides more room for the antisite defect than the 24*d* tetrahedral site. The issue of Ga site preference will be considered in more detail in Section 3.2. Nevertheless, importantly, it is evident from Table 1 that the antisite energies are lower for gallate garnets than they are for aluminate garnets by nearly 0.4 eV for both Lu^{3+} and Y^{3+}. From this result, we are able to confidently predict that the cation antisite defect concentration is higher in gallate garnets than in the aluminate garnets, which has been proposed by previous experimental studies [13, 14]. A simple explanation of this result is that the ionic radius of Ga^{3+} is larger and more similar to Lu^{3+} and Y^{3+} than Al^{3+} (0.62 Å vs. 0.535 Å, respectively, for VI-fold coordination [15]), resulting in less induced strain when forming an antisite defect.

Table 1 Calculated energies of cation antisite disorder reactions for YAG and YGG (and LuAG and LGG), where the left hand of the defect reaction is $RE_{RE} + Me_{Me}$ (RE denotes either Lu or Y and Me denotes either Al or Ga).

defect products	energy (eV)
$Y_{Al}^{16a} + Al_Y$	1.93
$Y_{Al}^{24d} + Al_Y$	2.51
$Y_{Ga}^{16a} + Ga_Y$	1.59
$Y_{Ga}^{24d} + Ga_Y$	2.13
$Lu_{Al}^{16a} + Al_{Lu}$	1.80
$Lu_{Al}^{24d} + Al_{Lu}$	2.00
$Lu_{Ga}^{16a} + Ga_{Lu}$	1.41
$Lu_{Ga}^{24d} + Ga_{Lu}$	1.89

We have also investigated the partial substitution of Al^{3+} by Ga^{3+} and the effect of solid solutions on antisite defect formation. For example, we have considered replacing all 16*a* Al^{3+} cations with Ga^{3+}, which can be expressed as $Lu_3Ga_2^{16a}Al_3^{24d}O_{12}$ or $Y_3Ga_2^{16a}Al_3^{24d}O_{12}$ (LuGAG and YGAG, respectively). This composition is particularly interesting as it was when 40% of the Al was substituted with Ga^{3+} that experimental studies observed an improvement in scintillator performance [11]. For these intermediate compositions, there are more possible antisite disorder reactions than the end member cases described in Table 1. For example, Table 2 describes the results of five antisite disorder reactions for both $Lu_3Ga_2^{16a}Al_3^{24d}O_{12}$ and $Y_3Ga_2^{16a}Al_3^{24d}O_{12}$. The observed trends for both compositions are similar. It is apparent that the lowest energy reaction is when Lu^{3+} and Y^{3+} are fixed on the 24*c* site and the 16*a* Ga^{3+} and 24*d* Al^{3+} swap sites. However, regarding scintillator performance, it is likely that Lu^{3+} and Y^{3+} on non-dodecahedral sites are more

Table 2 Calculated energies of cation antisite disorder reactions for $RE_3\,Ga_2^{16a}\,Al_3^{24d}O_{12}$, where the left hand of the defect reaction is $RE_{RE} + Ga_{Ga}^{16a} + Al_{Al}^{24d}$ (RE denotes either Lu or Y).

defect products	energy (eV)
$Ga_Y + Al_{Ga}^{16a} + Y_{Al}^{24d}$	1.45
$Ga_Y + Y_{Ga}^{16a} + Al_{Al}^{24d}$	1.47
$Y_Y + Al_{Ga}^{16a} + Ga_{Al}^{24d}$	0.32
$Al_Y + Ga_{Ga}^{16a} + Y_{Al}^{24d}$	2.66
$Al_Y + Y_{Ga}^{16a} + Ga_{Al}^{24d}$	1.52
$Ga_{Lu} + Al_{Ga}^{16a} + Lu_{Al}^{24d}$	1.30
$Ga_{Lu} + Lu_{Ga}^{16a} + Al_{Al}^{24d}$	1.32
$Lu_{Lu} + Al_{Ga}^{16a} + Ga_{Al}^{24d}$	0.31
$Al_{Lu} + Ga_{Ga}^{16a} + Lu_{Al}^{24d}$	2.48
$Al_{Lu} + Lu_{Ga}^{16a} + Ga_{Al}^{24d}$	1.44

responsible for trapping electrons than other types of antisite. For this reason, it is interesting to observe in Table 2 that most of the antisite disorder energies for these intermediate compounds are lower than any end member reaction.

The final antisite disorder mechanism we considered was for the composition where all 24*d* sites are occupied by Ga^{3+}, which can be expressed as $Lu_3Al_2^{16a}Ga_3^{24d}O_{12}$ or $Y_3Al_2^{16a}Ga_3^{24d}O_{12}$ (LuAGG and YAGG, respectively). As for the case where 40% of the Al^{3+} cations were replaced by Ga^{3+}, when 60% of the Al^{3+} cations are replaced by Ga^{3+}, there are five cation antisite disorder reactions, the results of which are given in Table 3. Again, several reactions are lower energy than the end member antisite disorder reactions. In fact, for this composition, we predict that there is an antisite reaction for which each cation can be shifted from its original lattice position (at the dilute limit) that is <1 eV. It is also immediately apparent from Table 3 that a reaction for both Lu^{3+} and Y^{3+} is negative, suggesting that it should occur spontaneously. This reaction has the Lu or Y

Table 3 Calculated energies of cation antisite disorder reactions for $RE_3\,Al_2^{16a}\,Ga_3^{24d}\,O_{12}$, where the left hand of the defect reaction is $RE_{RE} + Al_{Al}^{16a} + Ga_{Ga}^{24d}$ (RE denotes either Lu or Y).

defect products	energy (eV)
$Ga_Y + Y_{Al}^{16a} + Al_{Ga}^{24d}$	0.81
$Ga_Y + Al_{Al}^{16a} + Y_{Ga}^{24d}$	2.04
$Y_Y + Ga_{Al}^{16a} + Al_{Ga}^{24d}$	−0.33
$Al_Y + Y_{Al}^{16a} + Ga_{Ga}^{24d}$	2.02
$Al_Y + Ga_{Al}^{16a} + Y_{Ga}^{24d}$	1.67
$Ga_{Lu} + Lu_{Al}^{16a} + Al_{Ga}^{24d}$	0.69
$Ga_{Lu} + Al_{Al}^{16a} + Lu_{Ga}^{24d}$	1.82
$Lu_{Lu} + Ga_{Al}^{16a} + Al_{Ga}^{24d}$	−0.34
$Al_{Lu} + Lu_{Al}^{16a} + Ga_{Ga}^{24d}$	1.87
$Al_{Lu} + Ga_{Al}^{16a} + Lu_{Ga}^{24d}$	1.55

cation remaining on its original 24*c* dodecahedral site, but the Al^{3+} and Ga^{3+} cations swapping positions, the Ga^{3+} moving from the 24*d* tetrahedral site to the 16*a* octahedral site. Recalling that the Ga^{3+} cation is larger than the Al^{3+} cation, it is reasonable to expect that Ga^{3+} prefers the larger solution site. This explanation is especially valid in this situation, where both cations are trivalent and no charge compensation is required. However, previous experimental studies have suggested that the Ga^{3+} unexpectedly prefers the smaller tetrahedral 24*d* site [23, 24]. In the next section, we delve further into the matter of Ga^{3+} solution site preference.

3.2 Ga site preference As mentioned, previous experimental studies have suggested that Ga^{3+} preferentially occupies the 24*d* tetrahedral site in YAG [23, 24], which is different than the slight preference for the 16*a* octahedral site predicted by pair potential calculations, as well as what is expected from conventional ionic radius arguments. Nevertheless, complementary studies in a wider range of garnet compositions support this non-intuitive Ga^{3+} site preference. For example, Geller et al. [25] found that Ga^{3+} preferentially occupied the 24*d* tetrahedral site in isostructural $Y_3Fe_5O_{12}$ (YIG). A similar observation in Ga^{3+}-doped YIG was made by Fischer et al. [26]. Despite these observations, no explanation for the non-intuitive distribution of Ga^{3+} was provided. However, Geller et al. did point out a few interesting characteristics of Ga^{3+} compounds that are anomalous when compared to corresponding Al^{3+} and Fe^{3+} compounds. First, $REGaO_3$ perovskite compounds do not exist for $RE = Y^{3+}$, Sm^{3+}, and Gd^{3+}, while similar compounds do exist for Al^{3+} and Fe^{3+} (e.g., $GdAlO_3$) [27]. Second, Geller et al. also observed that although the ionic radii of Fe, Ga, and Al descend in that order, the largest RE garnet to exist for Fe is $Sm_3Fe_5O_{12}$ (i.e., $Nd_3Fe_5O_{12}$ does not exist), while for Ga the largest garnet is $Pr_3Ga_5O_{12}$ and for Al the largest is $Gd_3Al_5O_{12}$ [25]. In these cases, likely due to partial covalency [28], Ga^{3+} is not behaving according to simple ionic radius rules.

More recently, Nakatsuka et al. [24] proposed covalent Ga–O bonding in garnet as an explanation for Ga residing on the smaller tetrahedral site. They supported this hypothesis with lattice parameter data for compositions between YAG and YGG. That the lattice parameters for the intermediate compositions are smaller than what is expected from Vegard's Law [29] supports their explanation since the cation–cation repulsion will be relaxed. Figure 1 compares the experimental lattice parameter data (in the form of deviation from Vegard's Law) of Nakatsuka et al. [24] and Marezio et al. [23] with values we calculated with both pair potentials and DFT. For the pair potential and the "ordered" DFT calculations, all Ga atoms in the 40% Ga composition reside on the octahedral site, and all Ga atoms reside on the tetrahedral site for the 60% Ga composition. Separate DFT calculations for "disordered" Ga distributions were also performed, relying on the special quasi random structure (SQS) approach [30] for consideration of a random distribution of Ga. It is clear from Fig. 1 that both the

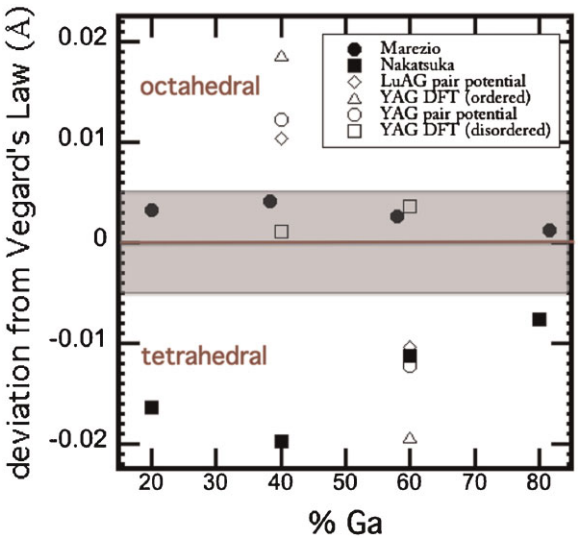

Figure 1 (online color at: www.pss-b.com) Comparison of calculated and experimentally (from Ref. [23, 24, 31]) measured lattice parameters of YAG and LuAG, shown as deviations from Vegard's Law. Positive deviations indicate an octahedral site preference of Ga, while negative deviations indicate an octahedral site preference. The red line indicates ideal Vegard's Law, the gray box suggests a limit (due to experimental error) within which compositions can be assumed to be obeying Vegard's Law.

Marezio and disordered DFT data have only very slight deviations from Vegard's Law. It is also clear that when the Ga atoms are forced to reside on octahedral sites, there is a positive deviation from Vegard's Law predicted by both pair potentials and DFT for YAG (and LuAG), which is evident from the results for 40% Ga. However, when the Ga atoms are forced to reside on tetrahedral sites (as is the case in the 60% composition), there is a negative deviation from Vegard's Law. This negative deviation is consistent with the data of Nakatsuka et al., which shows a consistent trend of intermediate compositions having a lattice parameter that was smaller than what was expected from Vegard's Law.

The DFT calculations also provide insight in to the energetics of site preference. To simulate the dilute limit, we put a single Ga atom at one of the Al sites in a 80- and 160-atom YAG supercell, respectively. According to our calculations, moving one Ga atom from tetrahedral site to octahedral site will cost an energy of 0.21 eV in both the 80- and 160-atom supercells. For the higher Ga doping levels, we find the total energy of the disordered configuration is $\approx$1.7 eV higher than that of the ordered configuration, suggesting that the preference of Ga atoms for tetrahedral sites persists also at non-dilute concentrations. Note that, the disordered configuration can be formed from an ordered configuration by "expelling" 10 Ga atoms from tetrahedral sites to octahedral sites. Thus, the "average" site-preference energy is obtained to be $\approx$0.17 eV per Ga atom, which is in good agreement with our dilute-limit calculations.

4 Summary In this paper, we have shown via atomistic simulations that the addition of Ga to $RE_3Al_5O_{12}$ garnets generally lowers the cation antisite defect formation energy, thus suggesting that Ga additions should lead to a higher concentration of antisite defects. This qualitative result supports previous studies that point to variations of the electronic structure (rather than defect concentration) as responsible for the improvement of garnet scintillator performance with Ga-doping. That is, Ga doping results in improved scintillator performance for Al garnets because of changes in the electronic structure and in spite of increases in antisite defect content. We have also shown that there is a tetrahedral site preference (over the octahedral site) for Ga occupation, and the impact of this site preference on the lattice parameter has been shown.

Acknowledgements We gratefully acknowledge partial support of Czech GACR P204/12/0805 project. Los Alamos National Laboratory, an affirmative action/equal opportunity employer, is operated by Los Alamos National Security, LLC, for the National Nuclear Security Administration of the U.S. Department of Energy under Contract No. DE-AC52-06NA25396.

References

[1] M. Kh. Ashurov, Yu. Voronko, V. V. Osiko, A. A. Sobol, and M. I. Timoshechkin, Phys. Status Solidi A **42**, 101 (1977).
[2] V. Lupei, A. Lupei, C. Tiseanu, S. Georgescu, C. Stoicescu, and P. Nanau, Phys. Rev. B **51**, 8 (1995).
[3] L. G. Volzhenskaya, Y. V. Zorenko, N. I. Patsagan, and M. V. Pashkovsky, Opt. Spectrosc. **80**, 135 (1987).
[4] M. Nikl, Phys. Status Solidi A **202**, 201 (2005).
[5] M. M. Kuklja, J. Phys.: Condens. Matter **12**, 2953 (2000).
[6] C. Milanese, V. Buscaglia, F. Maglia, and U. Anselmi-Tamburini, Chem. Mater. **16**, 1232 (2004).
[7] C. R. Stanek, K. J. McClellan, M. R. Levy, C. Milanese, and R. W. Grimes, Nucl. Instrum. Methods A **579**, 27 (2007).
[8] C. R. Stanek, K. J. McClellan, M. R. Levy, and R. W. Grimes, Phys. Status Solidi B **243**, R75 (2006).
[9] A. P. Patel, M. R. Levy, R. W. Grimes, R. M. Gaume, R. S. Feigelson, K. J. McClellan, and C. R. Stanek, Appl. Phys. Lett. **93**, 191902 (2008).
[10] M. Nikl, E. Mihokova, J. Pejchal, A. Vedda, Yu. Zorenko, and K. Nejezchleb, Phys. Status Solidi B **242**, R119 (2005).
[11] M. Nikl, J. Pejchal, E. Mihokova, J. A. Mares, H. Ogino, A. Yoshikawa, T. Fukuda, A. Vedda, and C. D'Ambrosio, Appl. Phys. Lett. **88**, 141916 (2006).
[12] M. Fasoli, A. Vedda, M. Nikl, C. Jiang, B. P. Uberuaga, D. A. Andersson, K. J. McClellan, and C. R. Stanek, Phys. Rev. B **84**, 081102(R) (2011).
[13] C. D. Brandle and R. L. Barns, J. Cryst. Growth **26**, 169 (1974).
[14] G. Shirinyan, K. L. Ovanesyan, A. Eganyan, A. G. Petrosyan, C. Pedrini, C. Dujardin, I. Kamenskikh, and N. Guerrassimova, Nucl. Instrum. Methods A **537**, 134 (2005).
[15] R. D. Shannon, Acta Crystallogr. A **32**, 751 (1976).
[16] M. Born, Atomtheorie des festen Zustandes (Teubner, Leipzig, 1923).
[17] R. Buckingham, Proc. R. Soc. A **168**, 264 (1938).

[18] R. W. Grimes and D. J. Binks, J. Am. Ceram. Soc. **76**, 2370 (1993).
[19] M. R. Levy, R. W. Grimes, and K. E. Sickafus, Philos. Mag. **84**, 533 (2004).
[20] C. R. A. Catlow and W. C. Mackrodt (Eds.), Computer Simulation of Solids (Springer-Verlag, Berlin, 1982).
[21] G. Kresse and J. Hafner, Phys. Rev. B **47**, 558 (1993).
[22] F. A. Kröger and H. J. Vink, Solid State Phys. (1957).
[23] M. Marezio, J. P. Remeika, and P. D. Dernier, Acta Crystallogr. B **24**, 1670 (1968).
[24] A. Nakatsuka, A. Yoshiasa, and T. Yamanaka, Acta Crystallogr. B **55**, 266 (1999).
[25] S. Geller, J. A. Cape, G. P. Espinosa, and D. H. Leslie, Phys. Rev. **148**, 522 (1966).
[26] P. Fischer, W. Hälz, E. Stoll, and A. Segmüller, Acta Crystallogr. **21**, 765 (1966).
[27] S. Geller and M. A. Gilleo, Acta Crystallogr. **10**, 239 (1957).
[28] S. H. Wei and S. B. Zhang, Phys. Rev. B **63**, 045112 (2001).
[29] L. Vegard, Z. Phys. **17**, 5 (1921).
[30] A. Zunger, S. H. Wei, L. G. Ferreira, and J. E. Bernard, Phys. Rev. Lett. **65**, 353 (1990).
[31] A. Nakatsuka, A. Yoshiasa, and S. Takeno, Acta Crystallogr. B **51**, 737 (1995).

